Journal of Power Sources 273 (2015) 174–179

Contents lists available at ScienceDirect

Journal of Power Sources

journal homepage: www.elsevier.com/locate/jpowsour

Polyacrylate bound $TiSb_2$ electrodes for Li-ion batteries

Juan Luis Gómez-Cámer*, Petr Novák

Paul Scherrer Institute, Electrochemistry Laboratory, CH-5232 Villigen PSI, Switzerland

HIGHLIGHTS

- The polyacrylate binder (PAA) improves the cycle life of $TiSb_2$ electrodes.
- The particle size of $TiSb_2$ influenced the rate capability keeping long cycle life.
- Cycling performance of improved $TiSb_2$ electrodes is demonstrated in full cells.

ARTICLE INFO

Article history:
Received 16 July 2014
Received in revised form
9 September 2014
Accepted 11 September 2014
Available online 18 September 2014

Keywords:
$TiSb_2$
Binder
Polyacrylate
Rate capability
Electrode engineering
Lithium batteries

ABSTRACT

Crystalline $TiSb_2$ electrodes prepared using two different binders, PVDF and lithium polyacrylate (LiPAA), were examined as negative electrodes in Li-ion batteries. The cycle life of the electrodes is strongly influenced by the choice of the binder, reaching ca. 120 cycles with LiPAA vs. ca. 90 cycles achieved with the common binder PVDF. Moreover, rate capability is improved using LiPAA binder. The reduction in $TiSb_2$ particle size is shown to influence the average practical specific charge at high charge/discharge rates. The reasons for this improvement are discussed and the optimized electrode was demonstrated in full Li-ion cells.

1. Introduction

Current progress in new energy technology applications, from portable electronics to electric vehicles, demands the development of high-capacity energy storage devices. Li-ion batteries are the best choice for many applications due to their high energy and power densities and long cycle life. Most of the commercial batteries use graphite-based negative electrodes, which has good cyclability and a theoretical specific charge of 372 mAh g^{-1}. Nevertheless, this specific charge is too low for high-energy requiring devices. Thus, many promising materials have been extensively investigated as possible replacement for carbonaceous materials in negative electrodes for Li-ion batteries [1]. Among them, Si, Sn, and Sb [1–3] are the most promising in terms of specific charge and energy density, however, these materials undergo huge volume changes upon cycling, which has a negative impact on their cycle life.

In the case of Sb, alloys with an inactive element towards lithium such as Cu [4,5], Mn [6], Ni [7], V [8], Ti [8,9], Nb [10], Fe [11] or Co [12–17], two inactive elements [18], two active elements [19–21] and both active and inactive elements [22–24], have been widely investigated. The observed better cyclability compared to the respective pure element is due to a fine dispersion of the inactive metal during cycling, which ensures good conductivity, or a multi-step lithiation in the case of alloying with other active metal, both resulting in a better buffering of the volume changes. Nevertheless, further improvement has been demonstrated being possible by engineering the electrodes. Particle size control can significantly improve the cycling performance of Sn and Sb based electrodes to around 100 cycles by using sub-micrometer or nanometer sized particles [25] but also electrolyte additives [26,27]. The combination of binder, commonly carboxymethyl cellulose (CMC), and additives [24,28] helps to reduce the irreversible charge losses due to SEI formation process and to enhance the cycle life of alloy-based electrodes. In the recent years polyacrylate based binders have been proposed for negative electrodes of Li-ion batteries. Thus, different polyacrylate salts have been explored in combination with graphite and compared to PVDF [29].

* Corresponding author. Tel.: +41 0563105770.
E-mail address: juan-luis.gomez@psi.ch (J.L. Gómez-Cámer).

http://dx.doi.org/10.1016/j.jpowsour.2014.09.087
0378-7753/

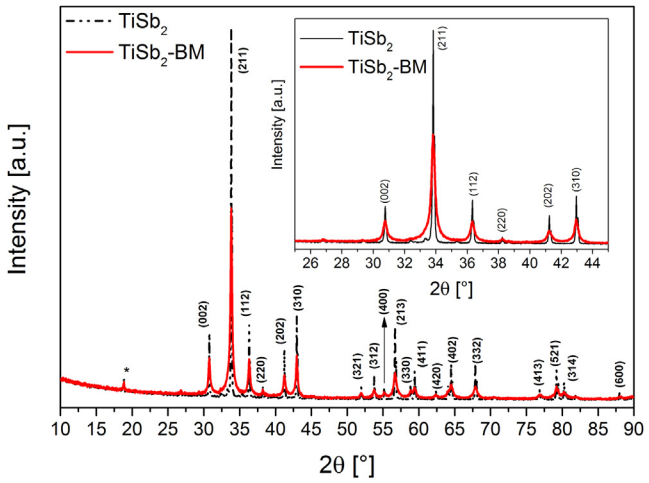

Fig. 1. X-ray diffraction patterns of pristine $TiSb_2$ and ball milled ($TiSb_2$-BM) samples. Inset: zoom indicating the peak broadening of the $TiSb_2$-BM sample.

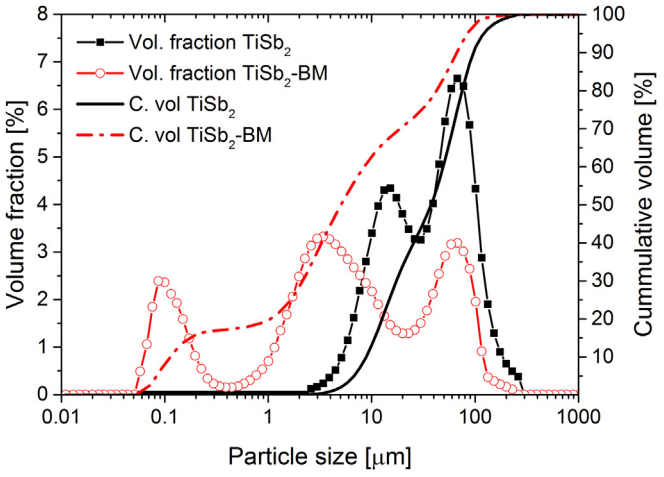

Fig. 3. Particle size distribution of the $TiSb_2$ and $TiSb_2$-BM samples.

Partially substituted polyacrylic acid has been demonstrated to improve the cycling performance of Si electrodes [30], and lithium polyacrylate was shown by Li et al. to perform better than PVDF and CMC in combination with a Sn–Co–C negative electrode [31]. In this work we investigate the $TiSb_2$ alloy as promising negative electrode for Li-ion batteries. In our previous communication we explored its reaction mechanism by means of *in situ* techniques [32]; here, a more detailed study of its electrochemical properties regarding the binder, particle size, and rate capability is presented.

2. Experimental

The $TiSb_2$ alloy was prepared by placing a mixture of the stoichiometric amounts of Ti (ABCR, Germany) and Sb (ABCR, Germany) metals in a tubular oven and heating them at 900 °C during 12 h under Ar atmosphere. After the heat treatment the sample was quenched by opening the tubular oven without stopping the Ar gas flow. After cooling down, prepared alloy was ground in a mortar prior to its use as active material for the negative electrode. $TiSb_2$ alloy samples with reduced particle size were prepare by the same procedure, followed by a ball milling step in a Fritsch Pulverisette 7 at 300 rpm during 8 h (hereafter $TiSb_2$-BM).

The crystal structure of the $TiSb_2$ alloys was characterized by X-ray diffraction (XRD) using a PANalytical Empyrean diffractometer equipped with a Cu Kα radiation source ($\lambda = 0.15406$ nm). SEM and post mortem SEM comparative analysis was performed using a Carl Zeiss UltraTM 55 scanning electron microscope operated at 5 kV in the in-lens secondary electron detection mode. Particle size distribution was measured by laser diffraction using a Horiba Partica LA-960 particle size analyzer.

For electrochemical testing, the $TiSb_2$ was mixed with Super P carbon black (Imerys, Switzerland) and a binder in a ratio of 80/10/10 weight percent and dispersed in the solvent using a POLYTRON® PT 2100 homogenizer (Kinematica AG) to form a viscous slurry. Two different binders were investigated in this study, 10 wt.% solution of PVDF Solef 1015 (Solvay, Belgium) in N-methyl pyrrolidone (NMP; Sigma–Aldrich, USA) and lithium polyacrylate (LiPAA, 12 wt.%) in water. The LiPAA solution was prepared by neutralizing a poly(acrylic acid) solution with lithium hydroxide. A stoichiometric amount of 10 wt.% $LiOH \cdot H_2O$ (Sigma–Aldrich) was added to 25 wt.% poly(-acrylic acid) (HPAA; Alfa Aesar, average M.W. 240.000) in a 1:1 molar ratio of LiOH to HPAA monomer. The mixture was adjusted to neutral pH and stirred during 8 h, resulting in a 12 wt.% LiPAA solution.

The electrode slurries were casted onto a copper foil via doctor blading and dried overnight at 80 °C under vacuum. Circular electrodes with diameters of 13 mm and a typical active mass of 5 mg were punched out, vacuum dried overnight at 120 °C, and assembled into coin-type cells in an argon-filled glove box. The reproducibility of the results was tested running a minimum of three electrodes per experiment. Glass fiber separators soaked in 1 M $LiPF_6$ in ethylene carbonate (EC)/dimethyl carbonate (DMC) electrolyte (1:1 by weight) were used. A lithium metal foil served both as counter and reference electrode. The cells were galvanostatically cycled between 50 mV and 1.5 V vs. Li^+/Li. Full cell experiments were performed using a positive electrode film of $Li(Ni_{0.33}Mn_{0.33}Co_{0.33})O_2$ (BASF SE, Germany).

3. Results and discussion

The $TiSb_2$ alloy which was synthesized by ceramic route from the elements exhibited a crystalline structure. All the peaks can be

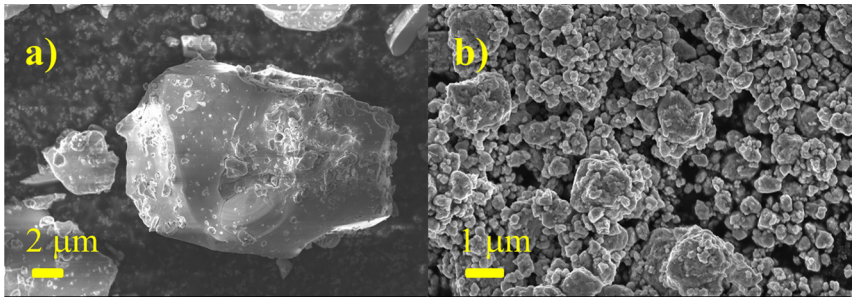

Fig. 2. SEM images of the pristine (a) as-synthesized $TiSb_2$ and (b) the ball milled $TiSb_2$ ($TiSb_2$-BM).

Table 1
Statistical data obtained from particle size measurements on the $TiSb_2$ samples.

Sample	Pristine $TiSb_2$ (μm)	Ball milled $TiSb_2$ (μm)
Mean	47.0	20.4
Mode	63.1	3.2
D10	8.9	0.1
D50	37.5	5.1
D90	97.0	66.5

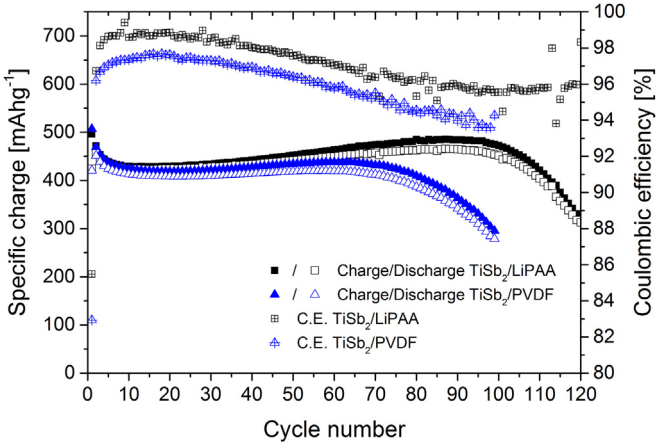

Fig. 4. Cycling behavior of $TiSb_2$ electrodes prepared with PVDF and LiPAA binder, respectively, cycled at 1C rate.

indexed in the tetragonal space group I4/mcm [32], as shown in Fig. 1. The as-synthesized material consists of large primary particles (Fig. 2a) that are often sintered in bigger agglomerates. The XRD shows that, after milling the alloy to reduce the particle size ($TiSb_2$-BM sample), the peaks were broadened but the crystalline structure was kept (Fig. 1). The ball milled sample consisted mainly of small particles (Fig. 2b), however, the particle size distribution compared to the parent pristine alloy was more inhomogeneous, as shown in Fig. 3. The average particle sizes were 47 and 20 μm for

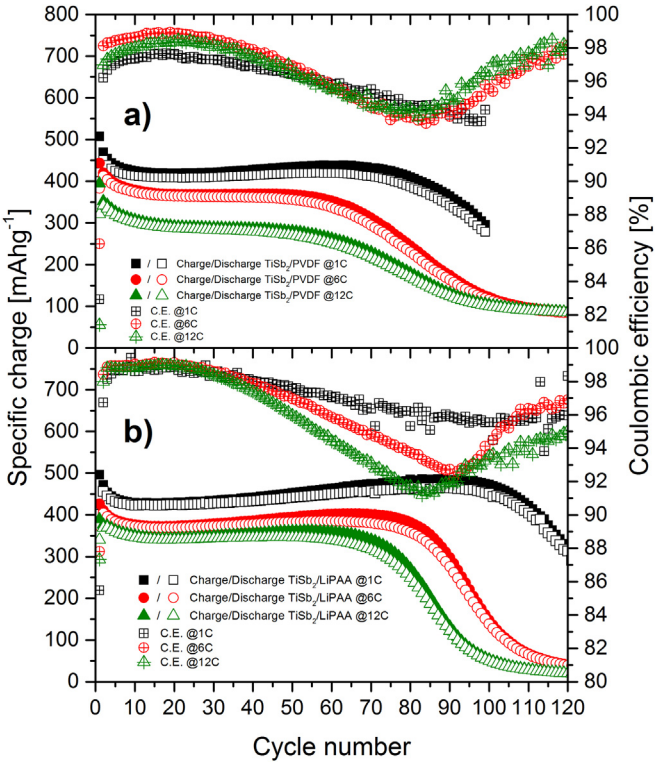

Fig. 6. Cycling behavior of (a) $TiSb_2$/PVDF electrodes and (b) $TiSb_2$/LiPAA electrodes cycled at 1C, 6C, and 12C.

$TiSb_2$ and $TiSb_2$-BM samples, respectively. However, comparing the mode sizes – the particle size of the largest number of particles – we see that the milled alloy consists mainly of particles of around 3 μm whereas the pristine $TiSb_2$ alloy contains the largest number of particles of about 63 μm. These results show that the ball milling process was effective in reducing the particle size. Further statistical details are summarized in Table 1.

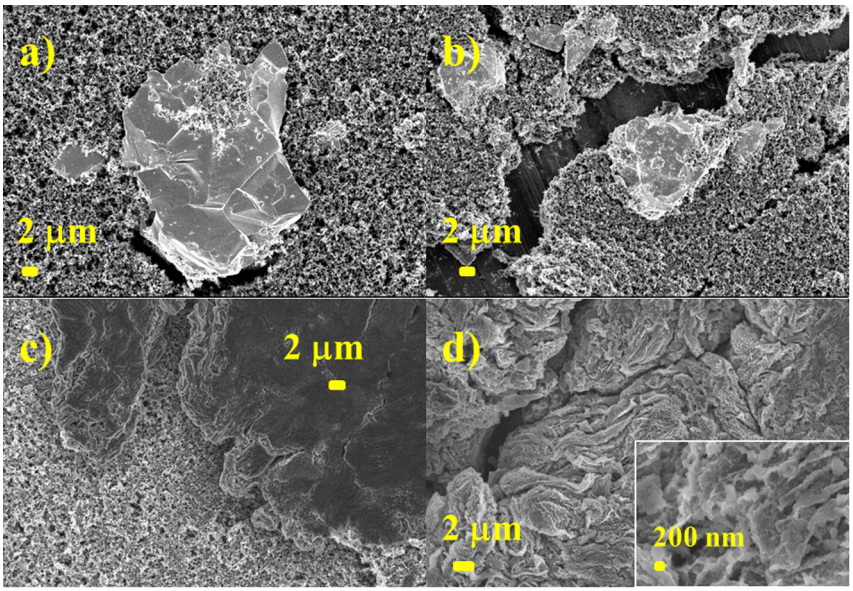

Fig. 5. SEM images of (a) pristine and (c) cycled $TiSb_2$/PVDF electrodes, and (b) pristine and (d) cycled $TiSb_2$/LiPAA electrodes. Inset in (d) corresponds to a higher magnification. The images of cycled electrodes were taken after 100 charge/discharge cycles.

Table 2
Practical specific charge, coulombic efficiency, and cycle life of $TiSb_2$ electrodes prepared with different binders and different particle sizes.

C-rate	Average specific charge [mAh g^{-1}]			Coulombic efficiency (1st/2nd cycle) [%]			Cycle life[a]		
	PVDF	LiPAA	BM/LiPAA	PVDF	LiPAA	BM/LiPAA	PVDF	LiPAA	BM/LiPAA
1C	420	420	440	83.0/96.0	85.5/96.5	86.5/98.0	85	115	110
6C	370	380	390	86.0/98.0	88.0/98.5	87.0/97.5	65	85	80
12C	300	350	370	81.5/97.0	87.5/98.0	87.0/98.0	50	75	75

[a] 80% of the specific charge in respect to the 2nd cycle.

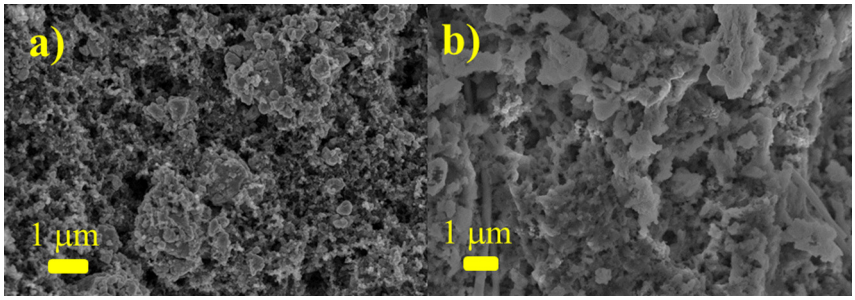

Fig. 7. SEM image of (a) pristine and (b) cycled $TiSb_2$-BM/LiPAA electrodes. Image of cycled electrode was taken after 100 charge/discharge cycles.

Fig. 4 shows a comparison of the cycling behavior of $TiSb_2$ electrodes with PVDF and LiPAA as a binder, cycled at 1C rate, i.e. 1 Li^+ per $TiSb_2$ in 1 h. Their specific charges were similar during the first ca. 60 cycles, over 420 mAh g^{-1}, but the fading after that point was faster for the PVDF based electrodes. The LiPAA based electrodes exhibited an extended cycle life maintaining more than 80% of the specific charge of the second cycle – according to the established criteria for the "end of life" – during ca. 115 cycles. On the contrary, PVDF based electrodes exhibited a cycle life of only ca. 85 charge/discharge cycles. It is worth to note that both electrodes exhibited a slight increase in specific charge during cycling with a slight decrease in coulombic efficiency, which is explained by the formation of a ternary phase, Li–Ti–Sb, which helps to stabilize the capacity in Sb-based alloys [32]. We hypothesize that the reason for the improved cycle life of the LiPAA based electrodes could lay in their higher charge/discharge efficiency during cycling, which reached more than 98% in the first 40 cycles and was still more than 96% until the end of their cycle life. On the other hand, PVDF based electrodes exhibited a coulombic efficiency of about 97% in the first 40 cycles, dropping then to values below 95% before rapidly losing cycling stability.

In order to shed some light on the differences between the $TiSb_2$ electrodes made with PVDF and LiPAA binders, comparative *post-mortem* SEM analysis was performed. Fig. 5 a and b shows the pristine electrodes prepared from $TiSb_2$ with PVDF or LiPAA binders, respectively. Both composite electrodes looked similar, with big $TiSb_2$ particles surrounded by much smaller carbon black particles. The only difference was the appearance of some cracks in the pristine film containing the LiPAA binder (Fig. 5b). After 100 charge/discharge cycles the electrodes had very different morphology. The cycled $TiSb_2$/PVDF electrode (Fig. 5c) exhibited a kind of "phase separation" between the carbon black, distinguishable in lighter color, and the mixture of Sb particles and Ti nanoparticles covered by a thick SEI film, in darker color. On the contrary, the cycled $TiSb_2$/LiPAA electrode (Fig. 5d) showed a good dispersion of Ti and Sb with the carbon black particles, which are undistinguishable even at higher magnification (cf. Fig. 5d, inset). Note that a better conductive additive dispersion improves the electron percolation in the electrode film, thus improving the rate capability.

Indeed, as can be seen in Fig. 6, at higher current densities the cycling properties of $TiSb_2$ electrodes prepared with PVDF and LiPAA binders were very different. For these tests, specific currents corresponding to 1C, 6C, and 12C were applied. The practical specific charge of PVDF based electrodes decreased from about 420 mAh g^{-1} (at 1C) to 370 mAh g^{-1} (at 6C) and 300 mAh g^{-1} (at 12C), which is consistent with kinetic effects of alloying reactions at high charge/discharge rates. The specific charge decrease was however less pronounced for the LiPAA based electrodes, maintaining roughly 380 mAh g^{-1} (at 6C) and 350 mAh g^{-1} (at 12C) compared to the ca. 420 mAh g^{-1} at 1C. It is worth noting that, in

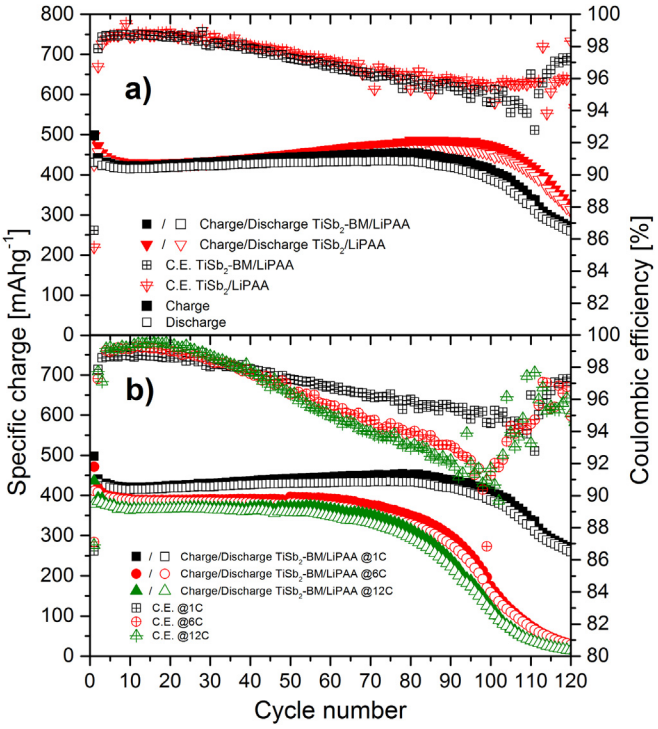

Fig. 8. (a) Cycling behavior of $TiSb_2$/LiPAA and $TiSb_2$-BM/LiPAA electrodes at 1C rate and (b) cycling behavior of $TiSb_2$-BM/LiPAA electrodes cycled at 1C, 6C, and 12C.

general, none of the electrodes at any C-rate exhibited a strong capacity fade, which indicates the effective buffering of volume changes exerted by the Ti nanoparticles matrix. Another interesting aspect is the high coulombic efficiency shown by the LiPAA based systems in the first 40 cycles even at high rates. Afterwards a clear trend can be observed: the higher the rate, the faster the fade in coulombic efficiency. Faster degradation of course results in shorter cycle life. Interestingly, an inversion point was observed in most of the coulombic efficiency curves, however we could not correlate it with the cycle life, shown in Table 2. We conclude that the use of the lithium substituted polyacrylate binder, LiPAA, improved the electrode homogeneity and conductive additive dispersion in the electrode films, favoring not only the rate capability of the $TiSb_2$ alloy, but also its coulombic efficiency.

In order to achieve further improvement in the electrochemical performance of $TiSb_2$ anodes, we tested the sample with reduced particle size ($TiSb_2$-BM, described in Figs. 1–3). The electrodes prepared from $TiSb_2$-BM alloy and LiPAA binder presented a similar morphology as the $TiSb_2$ electrodes with the same binder before and after cycling (Fig. 7). After 100 charge/discharge cycles the Sb, Ti, and the conductive additive particles were homogeneously dispersed. The similarities can be seen as well in the cycling behavior. In Fig. 8a the specific charges of $TiSb_2$ and $TiSb_2$-BM electrodes prepared with LiPAA binder are compared. Both electrodes delivered in general the same practical specific charge, however, the coulombic efficiency was higher in the first cycles for the ball milled sample. The lower efficiency exhibited by the larger active material particles could be related to the particle cracking upon lithiation, due to the large volume change. This process exposes new surface to the electrolyte, consequently consuming irreversibly Li^+ for SEI formation. Interestingly, coulombic efficiency for the milled sample is higher in the first 4–5 cycles, which might be due to a better management of the volume changes, therefore less particle cracking. The good cycling stability exhibited by both electrodes is mainly due to the presence of a ternary phase Li–Ti–Sb, which is demonstrated to help stabilizing the specific charge in this alloy [32]. The main difference between the $TiSb_2$ and $TiSb_2$-BM electrodes is the more stable specific charge values during cycling for the former. However both electrodes exhibited a similar cycle life of around 110 cycles.

The rate capability of the $TiSb_2$-BM sample was investigated and compared in Fig. 8b. As expected, reducing the active material's particle size enhances the rate capability due to shorter diffusion paths. As can be seen from Fig. 8b, the $TiSb_2$-BM electrodes can deliver about 440 mAh g^{-1} (at 1C), 390 mAh g^{-1} (at 6C), and 370 mAh g^{-1} (at 12C), exhibiting less capacity decay at higher rates than $TiSb_2$ electrodes prepared also with the LiPAA binder but having larger particle size. Both electrodes maintained similar cycle life.

The galvanostatic curves of the three $TiSb_2$ electrodes cycled at 1C, 6C and 12C are shown in Fig. 9. The $TiSb_2$ electrodes prepared from the pristine powder exhibited similar behavior in terms of

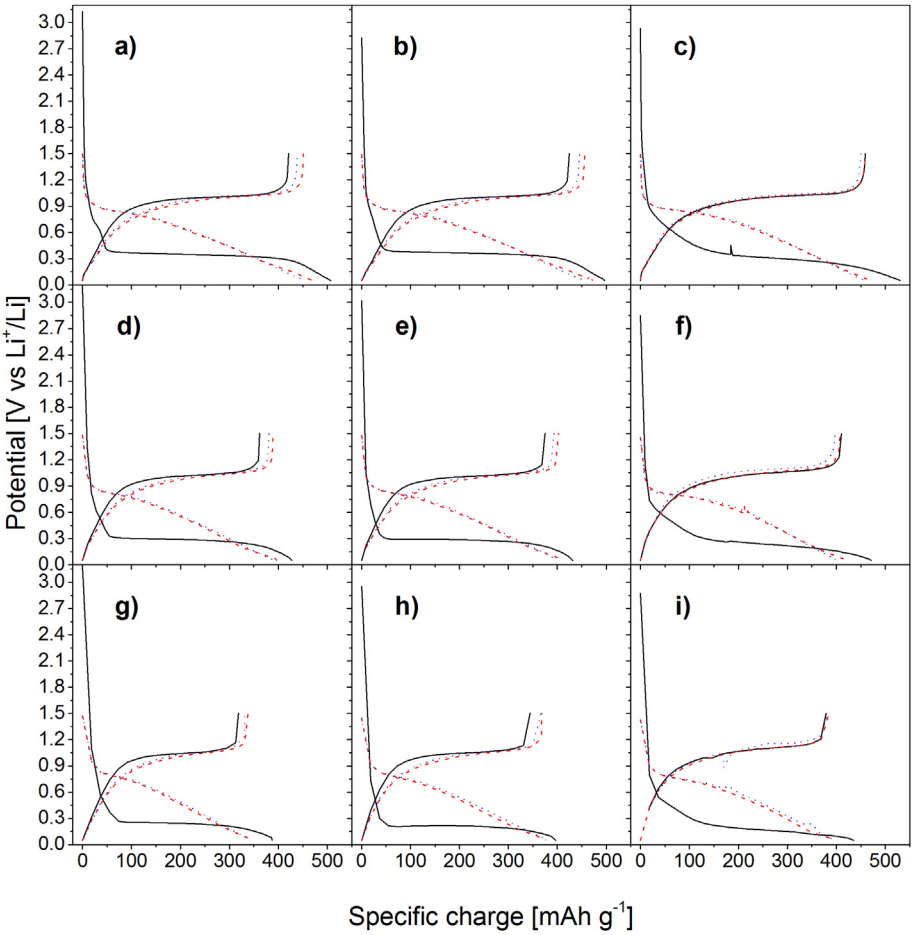

Fig. 9. Galvanostatic curves during the first (black solid line), second (red dashed line), and third (blue dotted line) cycles of the $TiSb_2$/PVDF electrodes at 1C (a), 6C (d), and 12C (g), the $TiSb_2$/LiPAA electrodes at 1C (b), 6C (e), and 12C (h), and the BM-$TiSb_2$/LiPAA at 1C (c), 6C (f), and 12C (i), respectively. (For interpretation of the references to color in this figure legend, the reader is referred to the web version of this article.)

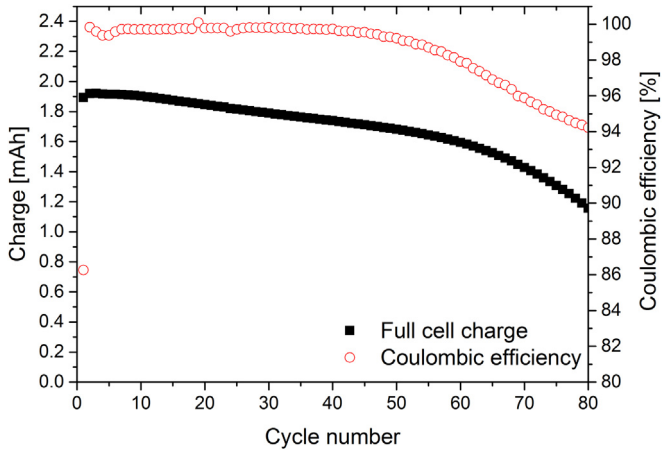

Fig. 10. Cycling behavior of $Li(Ni_{0.33}Mn_{0.33}Co_{0.33})O_2$/EC:DMC (1:1) 1 M $LiPF_6$/$TiSb_2$-BM full cells cycled at a specific current corresponding to 1C based on the anode active mass.

shape of the curves and irreversibility in the first three cycles at 1C, 6C and 12C. In the case of the BM-$TiSb_2$ sample, the galvanostatic curves were slightly different. In the first lithiation at 1C (Fig. 9c) a slope between 0.9 and 0.4 V can be seen before the plateau at ca 0.3 V. This region, according to our previous study of the reaction mechanism [32], corresponds to the insertion process into the $TiSb_2$ structure prior its conversion to Li_3Sb and Ti. The higher surface area of this sample, the more active material in contact with the electrolyte and the smaller is local current density, which favors the insertion reaction to take place to a larger extent, as it is visible at every C-rate (Fig. 9c, f and i). After the first lithiation, the irreversibility is smaller than for the electrodes made from pristine $TiSb_2$ and the course of the delithiation curves is identical from the first cycle, which is not the case for the pristine powder.

Under the light of these results we tested our optimized $TiSb_2$-BM/LiPAA negative electrode in full cells against a $Li(Ni_{0.33}Mn_{0.33}Co_{0.33})O_2$ positive electrode (Fig. 10). The voltage window was defined accordingly (4.0–2.0 V) and the current density was set to 1C based on the negative electrode mass. The positive/negative active mass ratio used to assemble the cells was calculated based on the criterion that the negative charge must be superior to that of the positive electrode in an extent of about 10%. This ensures on one hand the full utilization of the positive electrode and, on the other hand, despite some lithium is irreversibly consumed to build up the SEI film, the possibility of lithium plating due to overcharge is minimized. Nevertheless, Sb based alloys react with lithium at a potential, which is safely above that of metallic lithium. The full cells exhibited a charge of around 1.5 mAh per cm^2 of electrode area (absolutely 1.9 mAh) with a high coulombic efficiency over 99.5%, maintaining over 1.5 mAh after 70 cycles. Thus, the feasibility of the $TiSb_2$ negative electrodes was successfully demonstrated.

4. Conclusions

From the comparison of different $TiSb_2$ based electrodes, a clear improvement in rate capability, coulombic efficiency, and cycle life was observed when the electrodes were prepared with lithium polyacrylate (LiPAA) binder instead of the commonly used PVDF. The $TiSb_2$/LiPAA electrodes were able to maintain around 420 mAh g^{-1} for almost 120 cycles and showed improved cycle life at higher rates of more than a 30% compared to the PVDF bound electrodes. Reduction of particle size has been shown to play an important role at higher charge/discharge rates increasing the practical specific charge from ca. 350 to about 370 mAh g^{-1} at 12C and keeping the extended cycle life.

The optimized $TiSb_2$ electrodes with LiPAA binder and reduced particle size were electrochemically tested in full Li-ion cells using $Li(Ni_{0.33}Mn_{0.33}Co_{0.33})O_2$ as positive electrodes. The full Li-ion cells showed a stable cycling performance, with a cycle life close to 70 charge/discharge cycles until the limit of 80% of their original capacity was reached.

Acknowledgments

The authors are very grateful for the financial support from BASF SE.

References

[1] N. Nitta, G. Yushin, Part. Part. Syst. Charact. 31 (2014) 317–336.
[2] U. Kasavajjula, C. Wang, A. Appleby, J. Power Sources 163 (2007) 1003–1039.
[3] P.G. Bruce, B. Scrosati, J.-M. Tarascon, Angew. Chem. Int. Ed. 47 (2008) 2930–2946.
[4] L.M.L. Fransson, J.T. Vaughey, R. Benedek, K. Edström, J.O. Thomas, M.M. Thackeray, Electrochem. Commun. 3 (2001) 317–323.
[5] M. Morcrette, D. Larcher, J.M. Tarascon, K. Edström, J.T. Vaughey, M.M. Thackeray, Electrochim. Acta 52 (2007) 5339–5345.
[6] L.M.L. Fransson, J.T. Vaughey, K. Edström, M.M. Thackeray, J. Electrochem. Soc. 150 (2003) A86–A91.
[7] J. Xie, X.B. Zhao, H.M. Yu, H. Qi, G.S. Cao, J.P. Tu, J. Alloys Compd. 441 (2007) 231–235.
[8] D. Larcher, L.Y. Beaulieu, O. Mao, A.E. George, J.R. Dahn, J. Electrochem. Soc. 147 (2000) 1703–1708.
[9] C.M. Park, H.J. Sohn, J. Electrochem. Soc. 157 (2010) A46–A49.
[10] M.A. Reddy, U.V. Varadaraju, J. Power Sources 159 (2006) 336–339.
[11] J. Xie, X.B. Zhao, G.S. Cao, M.J. Zhao, Y.D. Zhong, L.Z. Deng, Mater. Lett. 57 (2003) 4673–4677.
[12] J. Yang, M. Wang, Y. Zhu, H. Zhao, R. Wang, J. Chen, J. Alloys Compd. 509 (2011) 7657–7661.
[13] J. Xie, X.B. Zhao, G.S. Cao, Y.D. Zhong, M.J. Zhao, J.P. Tu, Electrochim. Acta 50 (2005) 1903–1907.
[14] R. Alcántara, F.J. Fernández, P. Lavela, J.L. Tirado, J.C. Jumas, J. Olivier-Fourcade, J. Mater. Chem. 9 (1999) 2517–2521.
[15] J.M. Tarascon, M. Morcrette, L. Dupont, Y. Chabre, C. Payen, D. Larcher, V. Pralong, J. Electrochem. Soc. 150 (2003) A732–A741.
[16] J. Xie, X.B. Zhao, G.S. Cao, Y.D. Zhong, M.J. Zhao, J. Mater. Sci. Lett. 22 (2003) 221–224.
[17] J. Xie, X.B. Zhao, G.S. Cao, Y.D. Zhong, M.J. Zhao, J. Electroanal. Chem. 542 (2003) 1–6.
[18] L.J. Zhang, X.B. Zhao, X.B. Jiang, C.P. Lv, G.S. Cao, J. Power Sources 94 (2001) 92–96.
[19] H. Li, G. Zhu, X. Huang, L. Chen, J. Mater. Chem. 10 (2000) 693–696.
[20] J. Yang, Y. Takeda, N. Imanishi, T. Ichikawa, O. Yamamoto, Solid State Ionics 135 (2000) 175–180.
[21] H. Zhao, D.H.L. Ng, Z. Lu, N. Ma, J. Alloys Compd. 395 (2005) 192–200.
[22] H. Guo, H. Zhao, X. Jia, J. He, W. Qiu, X. Li, J. Power Sources 174 (2007) 92–926.
[23] M.T. Sougrati, J. Fullenwarth, A. Debedenetti, B. Fraisse, J.C. Jumas, L. Monconduit, J. Mater. Chem. 21 (2011) 10069–10072.
[24] H.A. Wilhelm, C. Marino, A. Darwiche, L. Monconduit, B. Lestriez, Electrochem. Commun. 24 (2012) 89–92.
[25] W.J. Zhang, J. Power Sources 196 (2011) 13–24.
[26] F. Martín, J. Morales, L. Sánchez, Chem. Phys. Phys. Chem. 9 (2008) 2610–2617.
[27] L. Chen, K. Wang, X. Xie, J. Xie, J. Power Sources 174 (2007) 538–543.
[28] N. Ding, J. Xu, Y. Yao, G. Wegner, I. Lieberwirth, C. Chen, J. Power Sources 192 (2009) 644–651.
[29] S. Komaba, K. Okushi, H. Groult, ECS Trans. 11 (2008) 63–70.
[30] Z.-J. Han, N. Yabuuchi, K. Shimomura, M. Murase, H. Yui, S. Komaba, Energy Environ. Sci. 5 (2012) 9014–9020.
[31] J. Li, D.-B. Le, P.P. Ferguson, J.R. Dahn, Electrochim. Acta 55 (2010) 2991–2995.
[32] J.L. Gómez-Cámer, C. Villevieille, P. Novák, J. Mater. Chem. A 1 (2013) 13011–13016.